

Journal Pre-proofs

Multi-level structured polylactic acid electrospun fiber membrane based on green solvents for high-performance air filtration

Jing Ge, Xujin Lv, Jianwei Zhou, Yarong Lv, Jingyi Sun, Han Guo, Ce Wang, Ping Hu, Zdenko Spitalsky, Yong Liu

PII: S1383-5866(23)02567-4
DOI: <https://doi.org/10.1016/j.seppur.2023.125659>
Reference: SEPPUR 125659

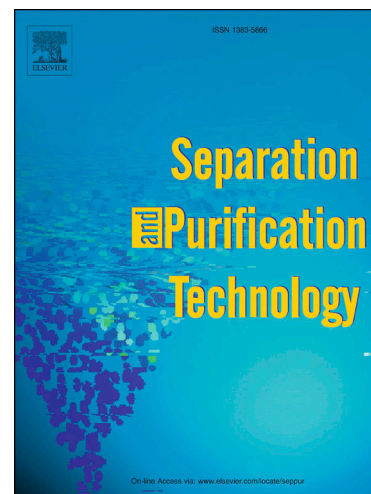
To appear in: *Separation and Purification Technology*

Received Date: 7 October 2023
Revised Date: 28 October 2023
Accepted Date: 7 November 2023

Please cite this article as: J. Ge, X. Lv, J. Zhou, Y. Lv, J. Sun, H. Guo, C. Wang, P. Hu, Z. Spitalsky, Y. Liu, Multi-level structured polylactic acid electrospun fiber membrane based on green solvents for high-performance air filtration, *Separation and Purification Technology* (2023), doi: <https://doi.org/10.1016/j.seppur.2023.125659>

This is a PDF file of an article that has undergone enhancements after acceptance, such as the addition of a cover page and metadata, and formatting for readability, but it is not yet the definitive version of record. This version will undergo additional copyediting, typesetting and review before it is published in its final form, but we are providing this version to give early visibility of the article. Please note that, during the production process, errors may be discovered which could affect the content, and all legal disclaimers that apply to the journal pertain.

© 2023 Published by Elsevier B.V.



Multi-level structured polylactic acid electrospun fiber membrane based on green solvents for high-performance air filtration

Jing Ge¹, Xujin Lv¹, Jianwei Zhou¹, Yarong Lv¹, Jingyi Sun¹, Han Guo¹, Ce Wang², Ping Hu³, Zdenko Spitalsky⁴, Yong Liu^{1*}

¹Beijing Key Laboratory of Advanced Functional Polymer Composites, College of Materials Science and Engineering, Beijing University of Chemical Technology, Beijing 100029, China

²Alan G. MacDiarmid Institute, Jilin University, Changchun, Jilin 130012, China

³Department of Chemical Engineering, Tsinghua University, Beijing 100084, China

⁴ Polymer Institute Slovak Academy of Sciences, Dubravska cesta 9, Bratislava 845 41, Slovakia

*** Corresponding Authors**

E-mail: yongliu@mail.buct.edu.cn.

Abstract

Particle matter (PM) pollution seriously threatens public health as it can combine with viruses and heavy metals to enter the human body and cause various diseases. Electrospun polymer fiber membranes, especially biodegradable materials such as polylactic acid, have great potential in PM filtration. However, most polylactic acid fiber membranes are imbalanced between filtration efficiency and resistance. Porous and bead-like fibers offer higher filtration efficiency and are expected to address these challenges with their larger specific surface area. Nonetheless, this structure may compromise the mechanical strength of the fiber membrane, thereby affecting the stability of gas purification and separation. Additionally, the significant volatilization of solvents during solution electrospinning can result in environmental concerns. Here, we prepared a double-layer filter with beads and cracks using a green mixed solvent of N, N-dimethylacetamide and dimethyl carbonate. The difference in the volatilization rate of mixed solvents increases the roughness of the membrane surface and enhances the adsorption of PMs. The structural difference between the two layers of membranes enables graded filtration of particles, further reducing pressure drop. Moreover, the entanglement at the interfaces enhances the mechanical properties of the bilayer membrane. It is worth mentioning that the design of the double-layer membrane improves the overall hydrophobicity and has practical application potential.

Keywords: Polylactic acid (PLA), Green solvent, Graded filtration, PM pollution, Beads

1. Introduction

The particulate matter pollution and its effects on public health have gained significant global attention[1]. In addition to adsorbing viruses and bacteria, particulate matters (PMs) can also adsorb heavy metals[2, 3], volatile organic compounds[4, 5] and enter the human body through the respiratory tract, leading to various diseases, including cancer[6-9]. Electrospun polymer fiber membranes have the advantages of high specific area, high porosity, and controllable fiber diameter and morphology, which have better particle interception and promote airflow, making them an effective choice for solving PM pollution[10]. However, electrospun fiber membranes also face some challenges, including solvent toxicity, non-degradability of polymers, high resistance, and unstable filtration.

Solvent toxicity and material degradation are urgent environmental issues that need to be addressed. Most studies utilize solution electrospinning involving toxic solvents, such as dichloromethane[11] and tetrahydrofuran. The environmental impact of solvent volatilization and residue cannot be overlooked, and there is an urgent need to investigate various solvents or combinations of solvents to ensure good solution state and sustainability of polymer solutions[12]. Polymer fiber membranes such as polyvinylidene fluoride[13] and polyacrylonitrile[14] have been widely studied for air filtration[15]. However, the non-degradability of traditional fiber filters allows them to accumulate in the natural environment and may become carriers of harmful substances, thereby damaging the ecology[16]. Consequently, biodegradable fiber membranes based on polylactic acid (PLA) will be more attractive in replacing traditional fiber

filters.

The main issues with filtration membranes are filtration resistance and stability. The research on PLA fiber membranes has an imbalance between pressure drop and filtration efficiency. Tang[17] utilized the advantages of electrospinning in situ polarization to co-spin bone-like nanocrystalline hydroxyapatite bioelectrodes with PLA, resulting in a filter membrane with a bimodal structure and enhanced dielectric and polarization properties, which enhanced the electrostatic capture of particles. Compared with pure PLA fiber membrane, the improved fiber membrane has a particle interception efficiency of 94.38% and an air resistance of 55 Pa at an airflow speed of 32 L/min. In addition, the unique chiral structure of PLA allows it to be made into piezoelectric filtration materials. Specifically, by controlling the rotation speed of the fiber collector and the injection speed of the spinning solution, poly (L-lactic acid) exhibits different macroscopic and molecular arrangements, resulting in different piezoelectric coefficients. The prepared piezoelectric filter fibers have the advantage of stable filtration performance[18, 19], but their air resistance needs to be reduced.

Researchers have prepared fiber membranes with various structures, such as spindle-like[20] and porous-like[21], through electrospinning to obtain efficient and low-resistance filtration membranes. Increasing the adsorption area of PMs improved the filtration efficiency without significantly changing the pressure drop. However, the impact of these structures on the mechanical strength of fibers is rarely mentioned. Holes and cracks on fibers may lead to a significant decrease in mechanical properties. And the mechanical strength of fiber membranes can ensure stable filtration

performance[20]. Although mechanical defects can be improved by preparing microcrystalline cross-linked structures between Poly (D-lactic acid) and poly (L-lactic acid)[21, 22] or by adding high-strength materials, the harsh solvent conditions[23] and complex processes required to achieve microcrystalline structures pose new challenges.

In this work, we selected a green mixed solvent, Dimethyl carbonate (DMC) and N, N-dimethylacetamide (DMAc), to prepare PLA electrospun membranes. We investigated the effects of solvent ratio and PLA mass fraction on the surface morphology of fiber membranes, as well as the filtration characteristics of various morphology fiber membranes. Combining fiber membranes with different filtration characteristics prepared a double-layer high-efficiency filter with improved mechanical strength, enhanced hydrophobicity, and low resistance. We conducted in-depth research on the effects of the structure of the double-layer membrane on mechanical and filtration performance, including filtration efficiency, pressure drop, and long-term PM filtration. A detailed analysis of the enhanced hydrophobic effect in this work was also conducted. This work is thought to offer guidance in achieving eco-friendly and effective preparation of electrospun fiber membranes.

2. Experimental

2.1 Materials

Poly(lactic acid (PLA) (4032D, Mw=160000) was purchased from Nature Works, Co., Ltd., USA. Dimethyl carbonate (DMC) (> 99%) and N, N-dimethylacetamide (DMAc) (> 99%) were purchased from Shanghai Macklin Biochemical Technology

Co., Ltd, China. All reagents were analytically pure and were not further purified. White skin-friendly non-woven fabric was purchased from Han Dun Medical Equipment, China.

2.2 Preparation of spinning solution

Prepare five solvents with different volume ratios (DMAc/DMC=1:9, 3:7, 5:5, 7:3, and 9:1). Add PLA at mass fractions of 12% and 14%. Name the solutions as follows: A1C9-12, A3C7-12, A5C5-12, A7C3-12, A9C1-12, A3C7-14, A5C5-14, based on the solvent ratio of DMAc/DMC and PLA addition amount. Specific operation: A total of 5 ml of mixed solvent was prepared, and its mass was recorded. The PLA powder was accurately weighed using an analytical balance (Lichen Technology, FA1004, China) and added to the mixed solvent. The mixture was stirred at 50 °C for 12 hours until the PLA was completely dissolved. The amount of PLA (W_1) was calculated according to formula (1), where W_s is the mass of the solvent, and W_t is the mass fraction of PLA.

$$\frac{W_1}{W_1 + W_s} = W_t \quad (1)$$

2.3 Electrospun PLA fiber membrane

The spinning solution was filled into a 10 ml syringe and pushed out at a rate of 1.5 ml/h through the injection pump. The spinning needle with an inner diameter of 0.84 mm was connected to a positive voltage of 15.5 KV, and the receiving drum was connected to a negative voltage of 5 KV. The drum speed was set at 120 r/min. The distance between the needle and the drum was 18 cm, and the relative humidity was maintained at $20 \pm 10\%$. The monolayer membrane was spun for 1.5 hours, 1 hour, 45 minutes, and 30 minutes, respectively. Bilayer membranes were prepared using A3C7-

12 and A5C5-14, and the three groups of membranes were named D-PLA-1, D-PLA-2, and D-PLA-3 based on different spinning time ratios ($A3C7-12/A5C5-14 = 1:2, 1:1,$ and $2:1$). The spinning time for all three groups of membranes was 45 minutes. Taking D-PLA-1 as an example, the specific operation included spinning A3C7-12 for 15 minutes, replacing the spinning solution with A5C5-14, and continuing spinning for 30 minutes to obtain a bilayer membrane. All fiber membranes were dried at room temperature for 24 hours to remove residual solvents.

2.4 Characterization and Testing - Monolayer membrane

Test the viscosity and conductivity of 7 solution groups using a rotary viscosity meter (Lichen Technology, China) and a conductivity meter (DDS-307A, Hangzhou Qiwei Instrument, China). After spraying gold onto an appropriately sized fiber membrane, observe the morphology using a field emission electron microscope (ZEISS Gemini 300, Germany). Image J was then used to measure the diameter of fibers and beads. Adobe Photoshop CS6 (PS) binarized the images, creating black-and-white images wherein the white part represents surface fibers and the black part denotes pores. MATLAB and PS were used to calculate the ratio of black pixels in the binary image (S7), from which the porosity of the fiber membrane was obtained[24, 25]. To determine the weight and thickness of a specific area ($2 \times 2 \text{ cm}^2$) of the fiber membrane, an analytical balance and micrometer (Deqing Shengtaixin Electronic Technology Co., Ltd, China) was utilized. These measurements were then used to calculate the average base weight (**Table S3**) of the fiber membrane.

A mask filtration performance tester (SC-FT-1702DYY, Shichen, China) was used

to measure the filtration efficiency and pressure drop of the PLA fiber membrane. The test particle used was NaCl, with a particle size ranging from 0.3 μm to 10 μm , and the flow rate was set at 32 L/min. Each group of fiber membranes was measured three times to obtain an average value, and the standard deviation was calculated. The quality factor (QF) of the fiber filter was then calculated using Equation (2) [26], where η represents the filtration efficiency, and ΔP represents the pressure drop. This equation allows us to assess the performance of the fiber membrane filter. The relative humidity during testing is $25 \pm 5\%$.

$$QF = -\frac{\ln(1-\eta)}{\Delta P} \quad (2)$$

2.5 Characterization and Testing - Double membrane

The cross-section of D-PLA-1, D-PLA-2, and D-PLA-3 fiber membranes was observed using a field emission electron microscope (ZEISS Gemini 300, Germany). The tensile strength of A5C5-14, A3C7-12, D-PLA-1, D-PLA-2, D-PLA-3 were measured by a universal tensile machine (Xinke Instruments, China), with a tensile rate of 5 mm/min and a sample size of 1 x 5 cm². The filtration efficiency and pressure drop tests are the same as those of single-layer membranes.

Water contact angle and filtration performance test in water mist environment

The water contact angle on the upper and lower sides of D-PLA-3 was measured using a contact angle tester (Chengde Dingsheng JY-82C, China). Use a spray can to spray water on both sides of D-PLA-3 and immediately test the filtration efficiency. Record the water evaporation time on the surface of the fiber membrane and test another filtration performance.

PM static filtration performance

Real PM pollution was simulated by burning mosquito coils in the device depicted in **Fig. S1**. Burn mosquito repellent incense as PMs until the PM counter (Lu Yi, infrared version, China) reading in one box reaches $999 \mu\text{g}/\text{m}^3$, a fiber membrane or non-woven fabric with an effective area of 94.985 cm^2 is placed in the middle of the two boxes. The initial PM concentration of the two boxes is recorded. After 10 minutes, it is measured again to characterize the static interception performance.

Long-term filtration performance

Long-term filtration performance is an experiment based on static filtration performance. The device shown in **Fig. S2** is used for testing, and the PM concentration in the box is greater than $999 \mu\text{g}/\text{m}^3$, recording the value when the reading starts to change and then recording the value every 2 minutes until the PM counter value decreases to the ambient value, cycle 5 times. After the PM cycle test, the filtration performance of the fiber membrane was tested again. Energy Dispersive Spectrometer (EDS) is used to observe fiber membranes' morphology and elemental changes before and after PM testing. The testing elements are C, O, Ca, and Si.

3. Results and Discussion

3.1 Solution Properties

The physical properties of polymer solutions, such as solubility, viscosity, and conductivity, jointly determine the structure and morphology of fibers[27], thereby affecting the filtration performance of fiber membranes. Due to the numerous ester

bonds present in its molecular structure, PLA does not readily dissolve in water but undergoes degradation[28-30]. Furthermore, PLA exhibits limited solubility in anhydrous ethanol[31] and can only be dissolved through organic solvents such as chloroform. During electrospinning, a large amount of solvent evaporates, so the sustainability of the solvent is also essential. By querying the GlaxoSmithKline Solvent Sustainable Development Guidelines[32], the green degree of mixed solvents was evaluated (S3). The results are shown in **Fig. 1a**. Compared to chloroform, dichloromethane (DCM), and N, N-dimethylformamide (DMF), the solvents DMAc and DMC used in this work have a higher green degree. The Hilbert parameters (δt) and Hansen combination parameters[33] are often used to represent the solubility of a polymer in a particular solvent. When the δt values of the polymer and solvent are similar, their solubility parameters are compatible, making it more likely for them to form uniform and stable solutions.

On the other hand, low-quality solvents with significant differences in δt may have poor solvating abilities for the polymer. In such cases, the polymer chains may become entangled, making it difficult to dissolve them entirely and leading to unstable solution states, such as aggregates, gels, or precipitation[34]. In this work, A1C9-12 and A3C7-14 are unstable. A1C9 has the lowest solubility for PLA among the five solvent combinations, as its solubility parameter values differ significantly from PLA ($\delta t_{(PLA)} = 21.73$, $\delta t_{(A1C9)} = 20.43$). The unstable solution state of A3C7-14 is due to the addition of PLA exceeding the solubility of the solvent.

Fig. 1b illustrates the measured viscosity and conductivity of seven sets of spinning

solutions. As the volume ratio of DMAc/DMC increases, the viscosity of PLA solution monotonically decreases, and the conductivity monotonically increases. The change in solution viscosity is mainly related to the interaction distance (R_a) and relative energy difference (RED) of the five solvent groups. The lower the R_a and RED (as shown in **Table S2**), the greater the solubility of the PLA in mixed solvent, and the corresponding solution viscosity is also relatively low. After increasing the mass fraction of PLA, the viscosity of the solution significantly increased. Although the viscosity of A3C7-14 (4180 mPa•s) was lower than that of A5C5-14 (4873 mPa•s), it could not maintain a stable solution state due to its low solubility. The increase in conductivity is a result of the combined effect of the dielectric constant and the conductivity of the solvent[35]. DMC has both a smaller dielectric constant and conductivity compared to DMAc. Therefore, increasing the volume fraction of DMAc leads to a solution with higher conductivity. In addition, the conductivity of the solution decreases with the increase of PLA mass fraction. The conductivity of A3C7-12 and A5C5-12 is 1 $\mu\text{s}/\text{cm}$ and 2 $\mu\text{s}/\text{cm}$, while the conductivity of A3C7-14 and A5C5-14 is 0.8 $\mu\text{s}/\text{cm}$ and 1.6 $\mu\text{s}/\text{cm}$, which should be caused by a decrease in the relative content of free solvents[36]. The increase in solution viscosity and the decrease in solution conductivity will lead to an increase in fiber diameter.

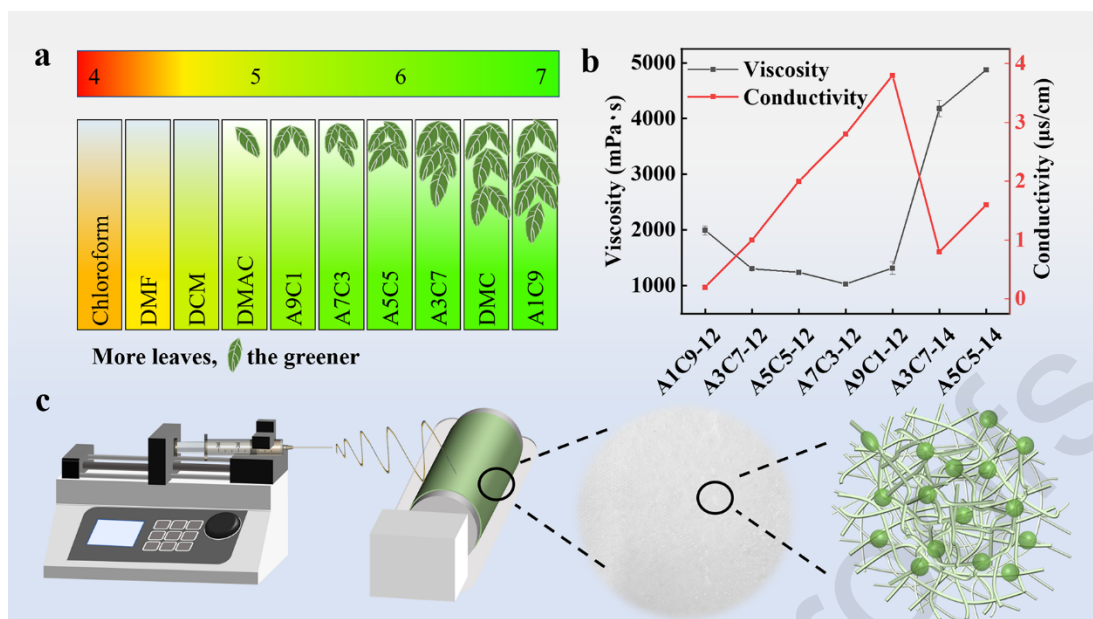


Fig. 1. (a) Green ranking of mixed solvents. (b) The viscosity and conductivity of solutions. (c) Schematic diagram of electrospinning device and PLA fiber membrane.

3.2 Micro morphology and porosity of monolayer membrane

The electrospinning device used in this article and the surface of the obtained fiber membrane are shown in **Fig. 1c**. PLA solution is sprayed from the tip of the syringe and randomly deposited on a drum with a skin-friendly, non-woven fabric. The SEM images in **Fig. 2** reveal that all seven groups of fibers exhibit varying degrees of bead-like structures. When the mass fraction of PLA is 12%, as the volume ratio of DMAc/DMC increases, the fiber diameter decreases from 96 nm to 26 nm. Simultaneously, the number of beads on the fiber increases, and the diameter of the beads decreases from 8.18 μm to 3.62 μm . These measurements are summarized in **Table 1**. The formation of beads can be explained as follows: when the viscosity of the solution is relatively low compared to the spinning system, the balance between the viscoelasticity, surface tension, and electrostatic repulsion of the jet becomes disrupted. This resulted in the formation and stability of Taylor cones being affected. The

continuity of the jet was difficult to maintain, which led to the formation of a string of beads[37].

When the solution conductivity is low and the viscosity is high, the electrostatic force is insufficient to stretch the molecular chains during the rapid evaporation of the solvent. Consequently, the shape of the bead increases and changes from a circular shape to a spindle shape[38] (as shown in **Fig. S5**). In addition, it was observed that the fibers of A5C5-12 and A7C3-12 exhibit a network structure. This is because the solutions of these two groups have higher conductivity and lower viscosity (**Fig. 1b**). During the leap process, the surface charge density of the jet increases and the viscosity decreases, a single jet will split into multiple fibers, and these split fibers will adhere to each other to form a fiber reticular structure[39, 40]. When the mass fraction of PLA increased to 14%, the fiber diameter in the A3C7 solvent increased from 84 nm to 271 nm, and the fiber diameter in the A5C5 solvent increased from 66 nm to 353 nm, which is directly related to the significant increase in solution viscosity. In addition, there are cracks on the surface of the fibers due to the difference in the volatilization rate of the mixed solvent, causing phase separation in the jet[41]. These cracks are similar to the structure of *Platyclus orientalis* (as shown in **Fig. 2**), and the surface area of the fibers will increase, providing more adsorption sites for PM[42], thereby improving the overall mechanical interception efficiency[43, 44].

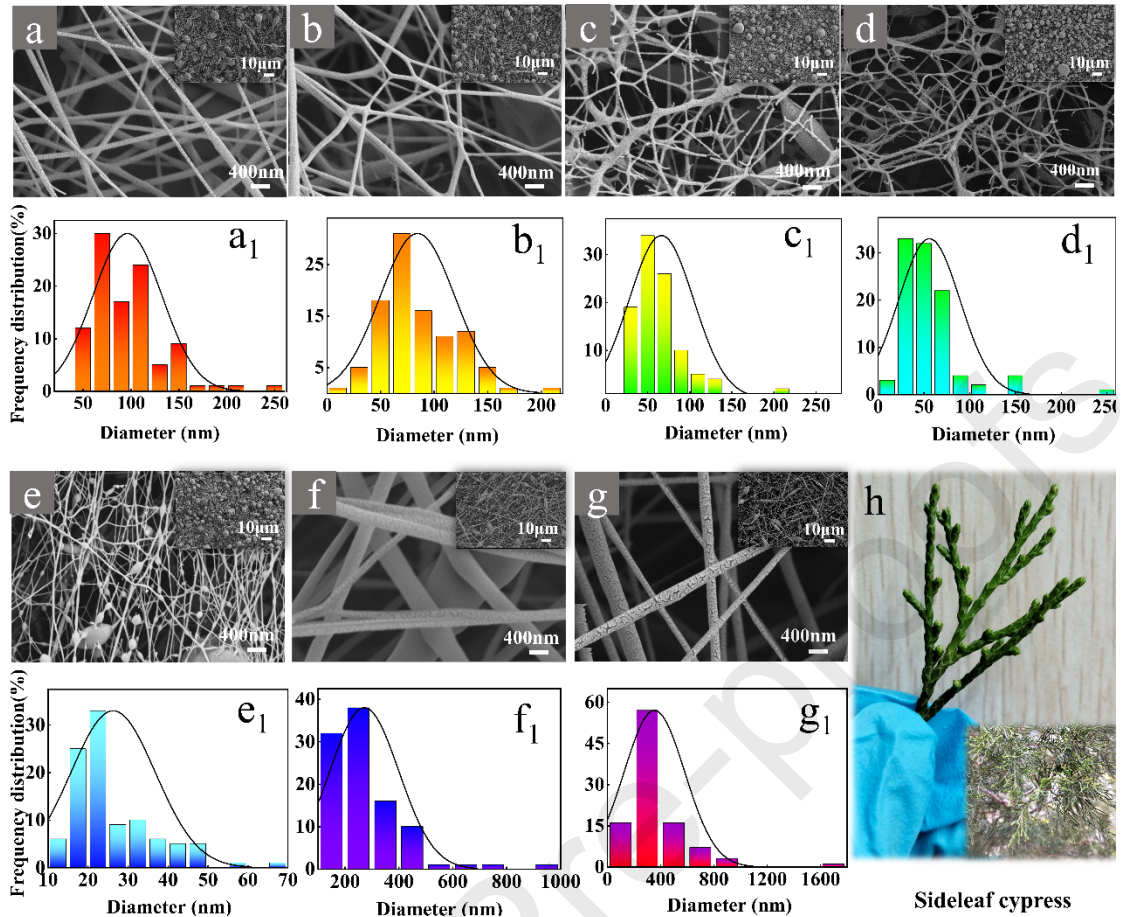


Fig. 2. SEM images and fiber diameter distribution of PLA fibers with different solvent combinations and PLA contents: (a) A1C9-12, (b) A3C7-12, (c) A5C5-12, (d) A7C3-12, (e) A9C1-12, (f) A3C7-14, (g) A5C5-14. (h) The morphology of greening plant side leaf cypress.

Table 1. Average diameter, bead diameter, and porosity of seven fibers.

Group	Average fiber diameter (nm)	Bead diameter (μm)	Porosity-PS (%)	Porosity-MATLAB (%)
A1C9-12	96.23 ± 35.87	8.18 ± 2.44	77.57 ± 1.44	76.68 ± 1.53
A3C7-12	84.41 ± 34.73	5.23 ± 1.29	81.28 ± 1.73	80.49 ± 1.83
A5C5-12	66.24 ± 38.11	4.20 ± 1.47	72.82 ± 1.69	71.26 ± 1.62
A7C3-12	55.80 ± 33.40	3.91 ± 1.23	84.86 ± 0.99	83.58 ± 1.27
A9C1-12	26.26 ± 10.78	3.62 ± 1.43	77.71 ± 1.14	75.99 ± 1.28
A3C7-14	271.6 ± 0.127	4.85 ± 1.90	90.36 ± 0.42	90.36 ± 0.42
A5C5-14	353.6 ± 0.226	7.07 ± 3.72	90.81 ± 1.46	90.81 ± 1.46

The morphology and diameter of fibers play a crucial role in determining the porosity of fiber membranes. In this study, binary images of the surface fibers of seven different groups of filter membranes were obtained using Photoshop, and the porosity

was calculated. The results, as shown in **Fig. 3**, indicate that the porosity of the fibers is below 85% when the mass fraction of PLA is 12%. This is mainly attributed to the smaller fiber diameter. Among these groups, A5C5-12 exhibits the lowest porosity (72%) due to its interconnected network structure, suggesting a higher pressure drop. Although the fiber and bead diameter of A1C9-12 is larger than A3C7-12, the contribution of too few beads to fiber fluffiness is insignificant, resulting in a smaller porosity than A3C7-12. The porosity of A5C5-14 and A3C7-14 has been greatly improved, reaching over 90%, indicating that the fiber diameter significantly impacts the porosity of the membranes. In conclusion, the particle size, stacking density, fiber diameter, and arrangement all play a role in the porosity of fiber membranes. Adequate porosity is vital for minimizing pressure drop in filter membranes.

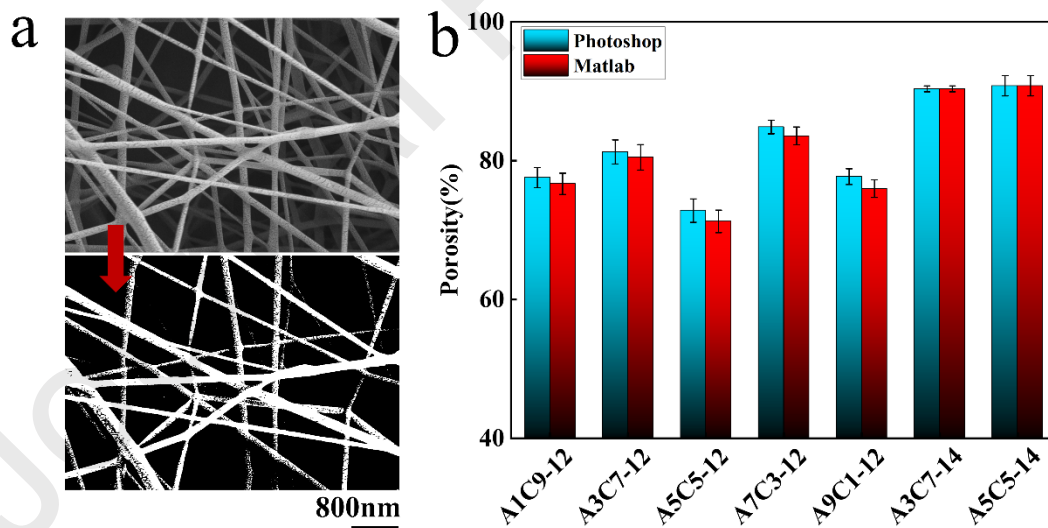


Fig. 3. (a) SEM images and their corresponding binary black and white images. (b) Porosity data of seven groups of fibers.

3.3 Filtration performance of monolayer membrane

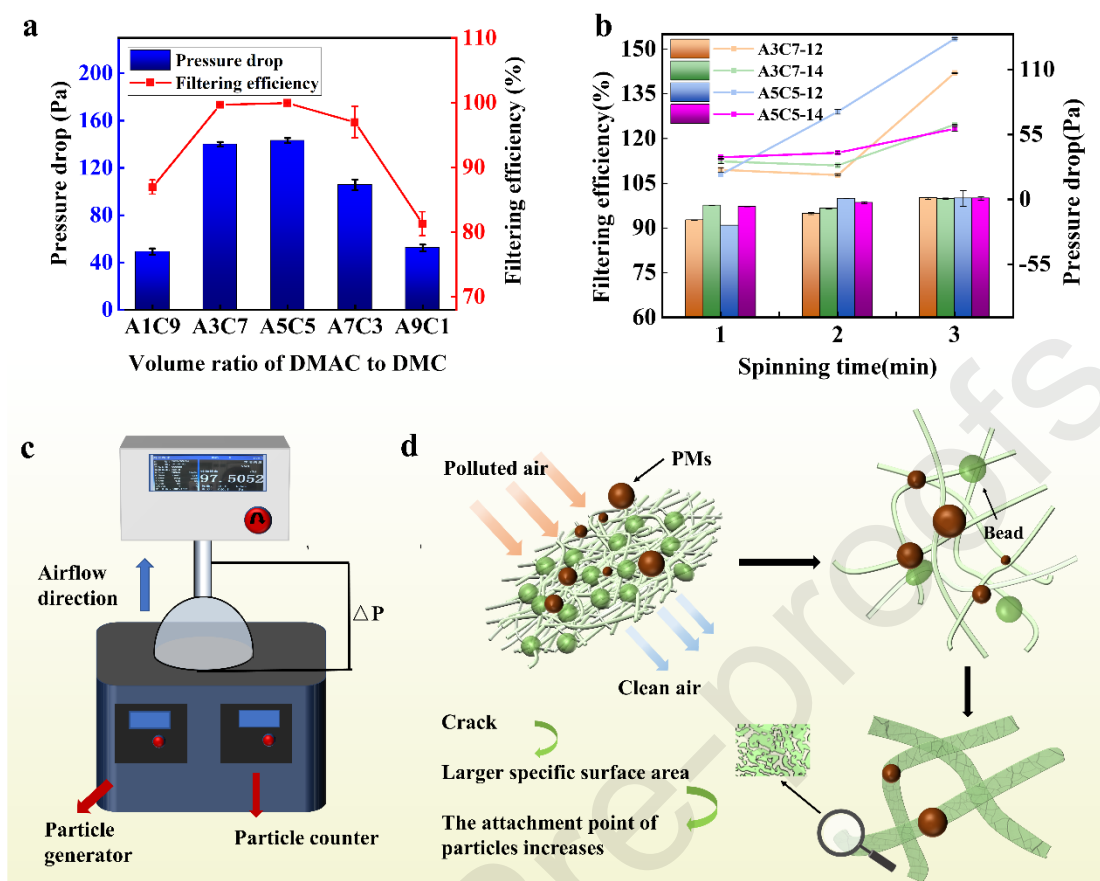


Fig. 4. (a) Filtering efficiency and Pressure drop of fiber membranes with a spinning time of 1.5 hours and a PLA mass fraction of 12%. (b) The corresponding filtration efficiency and resistance of four groups of fiber membranes at different spinning times, 1 - 30 minutes, 2 - 45 minutes, and 3 - 60 minutes. (c) Mask filtration performance tester. (d) Schematic diagram of the filtration process.

The device for filtering performance testing in this experiment is shown in **Fig. 4c**.

The filtration efficiency and pressure drop of fiber membranes with a PLA mass fraction of 12% and a spinning time of 1.5 hours are shown in **Fig. 4a**. The low filtration efficiency (86.93%) and pressure drop (49 Pa) in A1C9-12 can be attributed to the unstable solution state, which results in an uneven surface of the fiber membrane. On the other hand, A3C7-12 and A5C5-12 show filtration efficiencies above 99%. Filtration efficiencies of 96.96% and 81.25% are achieved by A7C3-12 and A9C1-12 respectively. By examining the SEM images and porosities, it can be inferred that A7C3-12 has an uneven pore distribution with more macropores, decreasing particle

interception efficiency. Likewise, the low filtration efficiency of A9C1-12 is attributed to its fine fibers, excessive beads, and weak fiber strength, which hinders effective particle interception. A7C3-12 also suffers from poor fiber strength. The interconnected mesh structure of A5C5-12 (99.63%, 154 Pa) results in a lower porosity than A3C7-12 (99.67%, 140 Pa), leading to slightly higher filtration efficiency and pressure drop.

To investigate the impact of spinning time and PLA addition on filtration efficiency, we selected A3C7 and A5C5 and prepared four sets of membranes: A3C7-12, A3C7-14, A5C5-12, and A5C5-14. The spinning time corresponds to the base weight of the fiber membrane (**Table S3**). As depicted in **Fig. 4b**, when the spinning time is reduced to 1 hour, the pressure drop of A3C7-12 and A5C5-12 decreases to 107 Pa and 136 Pa, respectively. However, A3C7-14 and A5C5-14 show lower pressure drops due to their high porosity (>90%), measuring 63 Pa and 59 Pa, respectively. Despite the decline in pressure drop, the filtration efficiency of all four membranes remains above 99%, with A3C7-12 achieving an impressive filtration efficiency of 99.99%. This indicates that simply increasing the base weight of the fiber membrane or reducing the fiber diameter to enhance filtration efficiency will result in a denser structure of the fiber membrane, leading to a higher pressure drop.

When the spinning time was further reduced to 45 minutes, a significant decrease in filtration efficiency and pressure drop was observed among the four groups of fiber membranes. Differences between the groups became more evident. The fiber membrane using A3C7 as the solvent showed a decrease in pressure drop to below 30 Pa and a decrease in filtration efficiency to below 96%. On the other hand, the fiber

membrane using A5C5 as the solvent maintained a filtration efficiency above 98% but with high resistance, measuring 74 Pa for A5C5-12 and 39 Pa for A5C5-14. When the spinning time was further reduced to 30 minutes, the filtration efficiency decreased but remained above 90% for all four groups of fiber membranes. The characteristic of maintaining high filtration efficiency while continuously reducing the base weight of the fiber membrane can be attributed to the presence of cracks and beads on the fiber surface. As shown in **Fig. 4d**, the cracks on the fiber membrane surface, caused by the difference in the volatilization rate of mixed solvents, increase the specific surface area of the fiber and enhance the probability of collision, sedimentation, and adsorption between the fiber and particles. The bead-like structure distributed on the fibers reduces the stacking density of the fiber membrane, facilitating airflow passage and reducing pressure drop. The fluffy fibers extend the particle motion path within the membrane, thereby increasing the probability of particle interception. Additionally, the fiber diameter plays a role in the porosity of the fiber membrane and its interception and collision with particles.

3.4 Cross-section morphology and tensile strength of double-layer fiber membranes

There is a lack of research on the mechanical properties of filter membranes, especially those with defective structures. Membranes with poor mechanical strength may not be able to sustain airflow and particle impact, thereby reducing filtration efficiency. **Fig. 5** reveals the cross-sectional morphology and tensile stress-strain curves of membranes. A3C7-12 and A5C5-14 were chosen because they have the best and

similar quality factors (**Fig. S7**). The tensile strength of single-layer fiber membranes is poor, below 0.8 MPa. A3C7-12 exhibits higher tensile strength and elongation at break than A5C5-14. It should be attributed to the presence of more beads in A3C7-12, which are interwoven with fiber bundles and can disperse the load during bearing capacity. The tensile strength of the three composite membranes has been greatly improved compared to single-layer membranes. With the increase of the A3C7-12 ratio, the double-layer membrane's tensile strength (**Table S4**) monotonically increases. The tensile strength of D-PLA-3 can reach 2.02 MPa. The gradual increase in tensile strength may be attributed to the entanglement of two layers of fiber membranes at the interface and the increased ratio of A3C7-12. As shown in the SEM image, the layered structure of the double-layer membrane is clearly visible, and the membrane is tightly adhered to each other.

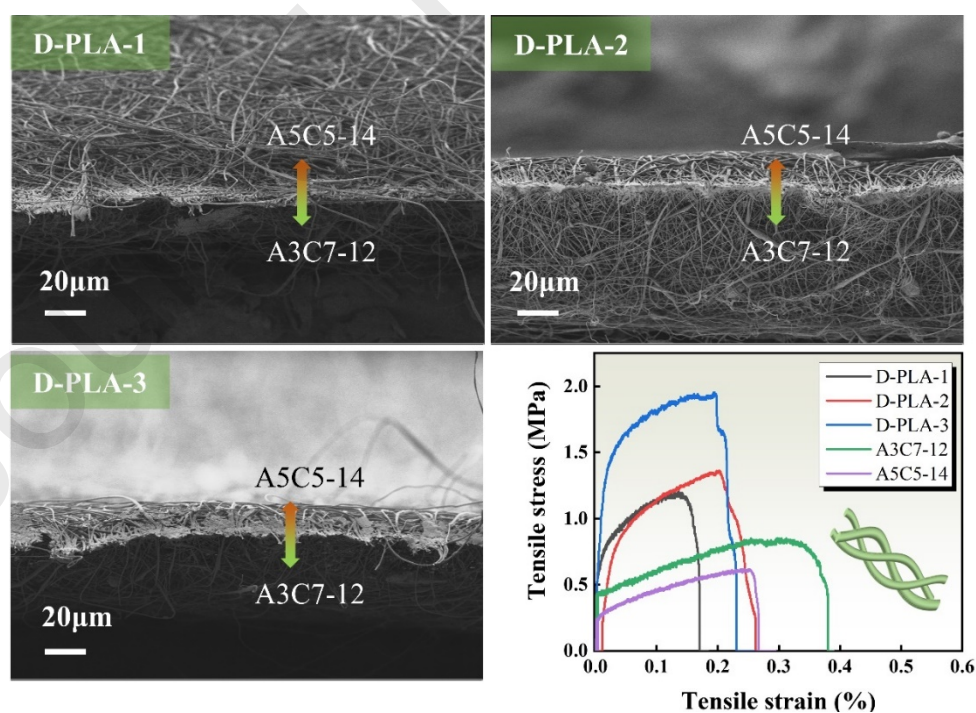


Fig. 5. The cross-sectional morphology and tensile stress-strain curve of the composite membrane.

3.5 Filtration performance of double membranes

3.5.1 Filtration performance at low humidity

Upon evaluating monolayer membranes for filtration efficiency, it was found that such membranes fail to maintain high efficiency under low-pressure drops[45, 46]. For instance, when the spinning time of A3C7-12 is set at 45 minutes, the resulting pressure drop is at 21 Pa, but the filtration efficiency is only at 94.83%. On the other hand, A5C5-14 achieves a filtration efficiency of 98.46% but with a relatively high-pressure drop of 39 Pa. The characteristics of the two sets of fiber membranes in terms of particle size filtration were analyzed and are shown in **Fig. 6a**. It can be observed that for particle sizes less than 2.5 μm , A3C7-12 demonstrates better particle filtration compared to A5C5-14. Conversely, for particle sizes greater than 2.5 μm , A5C5-15 performs better than A3C7-12. Both fiber membranes exhibit interception efficiencies above 90% for varying-sized particles. The different particle size filtration characteristics of two groups of fibers indirectly illustrate the role of fiber diameter in the collision interception of particles. Combining the two to prepare composite membranes can achieve graded filtration of particles[47, 48], thereby obtaining a filtration membrane with high efficiency and low resistance.

In the subsequent filtration tests, we conducted filtration on both sides of the double membrane, as shown in **Fig. 6b**. Based on the airflow direction, we categorized the fiber membrane into two sides: F and C. C represents the airflow passing through A5C5-14 first. At the same time, F means passing through A3C7-12 first. Interestingly, the three

membranes exhibited the same pattern, with the filtration efficiency of the C-side being higher than that of the F-side. This can be explained by the fact that larger particles are intercepted first when the C-side is used as the front end of the filter, while smaller particles are retained at the back end for further interception. The clear division of labor between the two layers of fibers results in higher filtration efficiency, as shown in **Fig. 6e**. On the contrary, fine fibers are not as effective in intercepting larger particles, and the continuous impact of particles on the fiber membrane increases the chances of particles passing through, resulting in lower filtration efficiency.

The average filtration efficiency values for the C-side of the three groups of membranes are 98.94%, 97.55%, and 98.02%, respectively, with corresponding average resistance values of 37 Pa, 53 Pa, and 31 Pa. The double-layer membrane achieved lower airflow resistance at the same filtration efficiency (98%). The high resistance of D-PLA-2 may be attributed to the uneven thickness of A3C7-12, which is locally too thick and causes airflow obstruction. Their quality factors are shown in **Fig. 6c**. Comparing the filtration performance of D-PLA-3 with commercial surgical masks and N95 masks at a test flow rate of 32 L/min (**Fig S8**), it was found that D-PLA-3 showed higher filtration efficiency (98.01%) and lower pressure drop (98.01%, 31.37 Pa) than N95 masks (96.79%, 54.21 Pa). Additionally, the filtration efficiency of D-PLA-3 and surgical masks was similar, both around 98%, with a pressure drop of 1.66 Pa lower than surgical masks. Finally, D-PLA-3, which had the lowest resistance and the highest average quality factor (0.12 Pa^{-1}), was selected for further experiments.

3.5.2 High humidity filtration performance

To simulate the filtering effect of the filter in a high humidity environment caused by human exhaled water vapor, a small spray can be used to spray water on both sides of D-PLA-3, with side C as the front end of the filter, and immediately tested. The results are shown in **Fig. 6d**, and after spraying water, the pressure drop of the fiber membrane increased significantly, from 31 Pa to 41 Pa. The filtering efficiency slightly decreased, from 98.02% to 97.94%. After the water vapor on the surface of the fiber membrane evaporates rapidly (3 minutes), the resistance returns to its original value. Water contact angle testing was conducted on both sides of the composite filtration membrane. The water contact angle on the A5C5-14 surface was 124 °, and the water contact angle on the A3C7-12 surface was 130 ° (**Fig. S9**). Both sides were hydrophobic materials, but A3C7-12 showed rapid absorption characteristics during testing, which can be attributed to the wicking effect of ultrafine fibers[49, 50].

The entire filtration process can be described as follows: During water spraying, a considerable quantity of liquid droplets accumulates at the front of the filter, obstructing the pores on the surface of the fiber membrane. This creates a convoluted and intricate airflow pathway at the micro-scale, causing increased resistance[51]. However, due to the hydrophobicity of the fiber surface, a portion of the droplets will evaporate (**Fig. 6f**). At the same time, the rest will be absorbed due to the F-side wicking effect, which exhibits hydrophobic properties and behaves like a lotus leaf. Additionally, the bead on the F-side mimics the structure of spider silk, creating differences in Laplacian pressure[52, 53] and surface energy gradient. This causes the droplets to be transported

to the beads directionally and then dropped (**Fig. 6f**). The expression for Laplace pressure (ΔP) [54] can be written as follows:

$$\Delta P = 2\gamma\left(\frac{1}{R_1} - \frac{1}{R_2}\right) \quad (3)$$

Among them, R_1 and R_2 are the local radii at both ends of the droplet, γ is the surface tension of water. In **Fig. 6f**, the radius of R_2 is greater than R_1 , which means that the Laplace pressure near the spindle knot is less than the joint. The nonequilibrium pressure difference will drive the droplet to transport towards the spindle knot. α and θ represent the backward and forward contact angles of water droplets on fibers. Spindle knots composed of random nanofibers typically have higher surface energy and smaller contact angles than joints composed of axially parallel nanofibers. The surface energy gradient force caused by differences in surface roughness causes water droplets to move from joints with poor hydrophilicity to spindle knots with higher wettability [54]. Considering these factors, the resistance of the fiber membrane has returned to its original value.

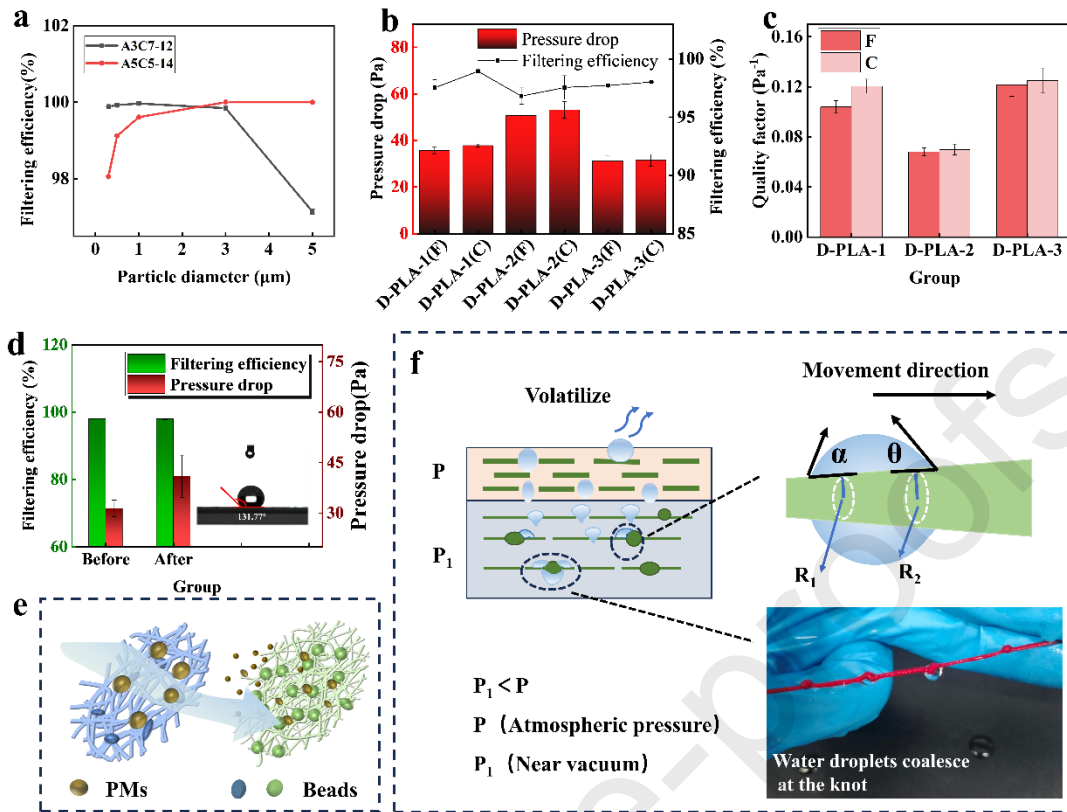


Fig. 6. (a) The filtration characteristics of A3C7-12 and A5C5-14 for particles with different particle sizes. (b) Double-sided filtration effect and pressure drop of composite membranes. (c) Quality factor of the composite film. (d) Filtration properties and water contact angle of D-PLA-3 before and after water spraying. (e) Schematic diagram of graded filtering. (f) Schematic diagram of core suction effect, lotus leaf effect, and Laplace pressure of composite membranes.

3.6 PM filtration performance

The static PM filtration performance of the fibers was characterized using the schematic diagram of the device shown in **Fig. S1**. Mosquito-repellent incense was burned in the transparent box on the left until the PM concentration exceeded $999 \mu\text{g}/\text{m}^3$. The PM concentration in the mosquito incense free box was recorded at the beginning and again after 10 minutes. The PM_{2.5} concentration in the non-filtration membrane group increased from $36 \mu\text{g}/\text{m}^3$ to $84 \mu\text{g}/\text{m}^3$, and the PM₁₀ concentration increased from $47 \mu\text{g}/\text{m}^3$ to $110 \mu\text{g}/\text{m}^3$. On the other hand, the PM_{2.5} concentration of the filtration membrane (D-PLA-3) group only increased from $29 \mu\text{g}/\text{m}^3$ to $30 \mu\text{g}/\text{m}^3$, and the PM₁₀ concentration increased from $38 \mu\text{g}/\text{m}^3$ to $39 \mu\text{g}/\text{m}^3$, indicating that the

filtration membrane had excellent static PM interception performance.

The long-term PM filtration performance of the fiber membrane was tested using the device shown in **Fig. S2**. Mosquito repellent incense was burned, causing the PM concentration inside the box to exceed $999 \mu\text{g}/\text{m}^3$ (which is far above the PM standard range). After 250 minutes of high PM pollution cycle testing, the filtration efficiency of the D-PLA-3 showed a slight decrease from 98.02% to 96.66%, with a resistance of 32 Pa. This decrease in efficiency is speculated to be due to the accumulation of particles and reduction in surface charge. The PM cycle test curves of D-PLA-3 are shown in **Fig. 7a,b**.

The surface morphology of the fibers was observed after the filtration cycle experiment, and the content and distribution of C, O, Ca, and Si were measured using EDS spectroscopy. The sandalwood and clay in mosquito repellent incense contain Ca and Si elements, while the fiber membrane before filtration does not. In the semi-quantitative analysis results of elements (**S13** and **Fig. 7e**), the filtered fiber membrane exhibited small particle aggregation, as depicted in **Fig. 7c**. This aggregation is visible as a bright purple color in **Fig. 7d**, indicating that the aggregates consist of mosquito repellent incense particles. The EDS spectrum results showed (**Fig. 7d**) that these elements were evenly distributed on the surface of the fiber membrane, demonstrating the particle interception effect of the fiber membrane. This indicates that the rough surface of the fiber membrane we prepared can effectively and uniformly intercept PM.

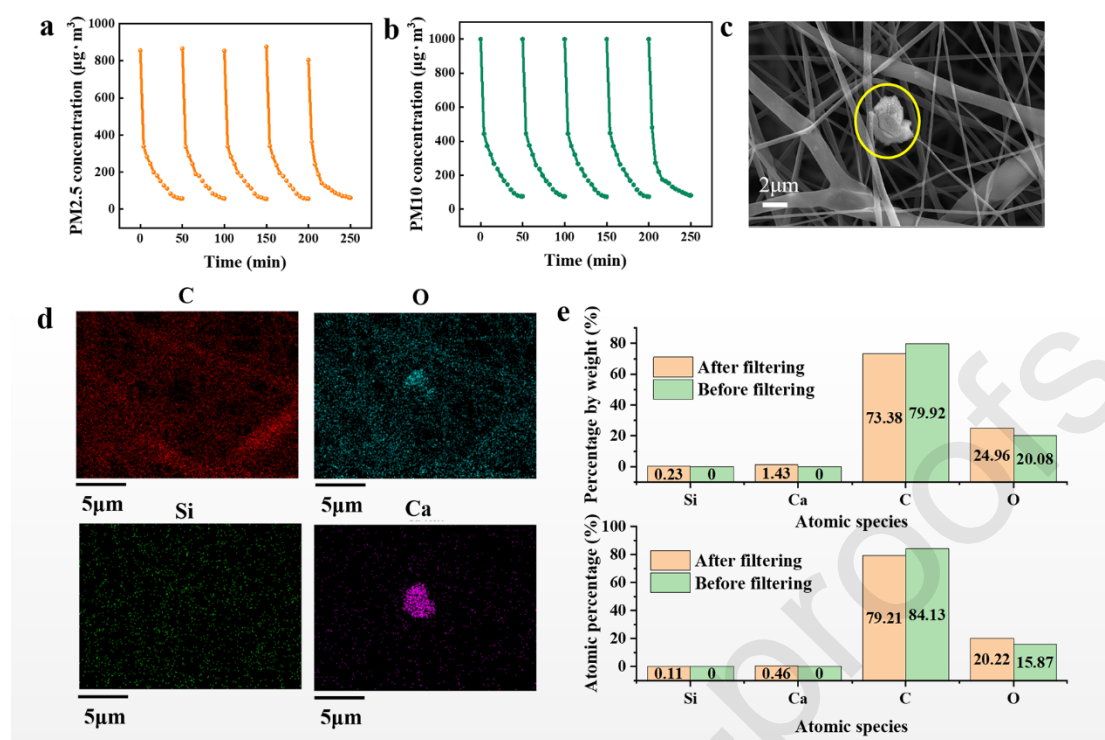


Fig. 7. Dynamic cycle curve of (a) PM2.5 and (b) PM10. (c) SEM image after PM filtration. (d) EDS element distribution diagram after PM filtration. (e) Atomic percentage and weight percentage of four elements of C, O, Si, and Ca on the fiber membrane after PM filtration.

4. Conclusion

This article uses green mixed solvent DMC/DMAc and degradable PLA materials to prepare electrospun fiber membranes for air filtration. DMC/DMAc mixed solvent displays a favorable blend of environmental friendliness and solubility, making it more eco-friendly compared to chloroform and more efficient in dissolving PLA than anhydrous ethanol. These materials allow for creating a surface rough fiber membrane with beads, thanks to the differences in volatilization rate and dielectric constant between the solvents. The presence of cracks on the fiber surface increases the surface area of the membrane, improving particle interception efficiency. Additionally, the presence of beads increases the distance between adjacent fibers, reducing pressure

drop and improving filtration efficiency by creating a more tortuous movement path for particles within the membrane. Based on these findings, a double-layer filter with a pore size gradient was designed and prepared. The layered structure of coarse and fine fibers enables graded filtration of particles. Optimization achieved particle removal efficiency of over 98% and a low-pressure drop of 31 Pa. The infiltration winding between the interfaces also increased the tensile strength of the fiber membrane.

Furthermore, this hydrophobic membrane exhibited enhanced moisture permeability by combining the lotus leaf and core suction effects. After cycling for 250 minutes under high PM pollution conditions, the filtration efficiency decreased by 1.36%, and the pressure drop increased by 1 Pa. This highlights the potential application of this green and environmentally friendly double-layer filter.

Declaration of Competing Interest

The authors declare that they have no known competing financial interests or personal relationships that could have appeared to influence the work reported in this paper.

Data availability

Data will be made available on request.

Acknowledgments

This work was supported by the National Natural Science Foundation of China (No. 21374008) and the Slovak Research and Development Agency under the contract (SK-CN-21-0010).

Declaration of generative AI and AI-assisted technologies in the writing process

During the preparation of this work the authors used none AI or AI-assisted technologies. The authors take full responsibility for the content of the publication.

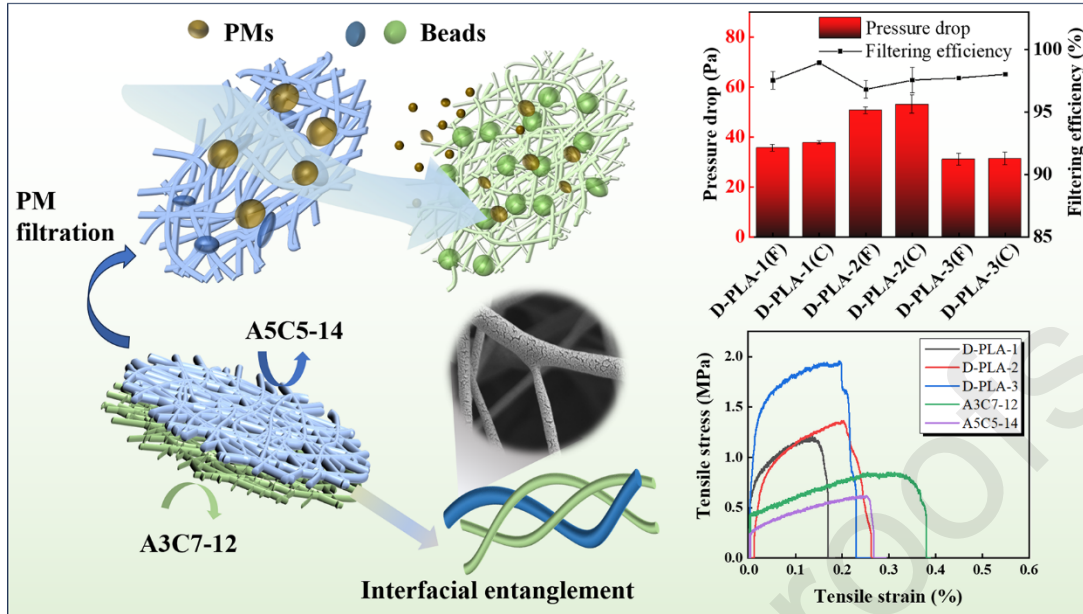
References

- [1] B. Furlow, Scientists call for US EPA to reconvene expert panel on particulate matter pollution, *The Lancet. Resp. Med.*, 7 (2019) 737-738. [https://doi.org/10.1016/S2213-2600\(19\)30221-8](https://doi.org/10.1016/S2213-2600(19)30221-8)
- [2] N. Kappelt, H.S. Russell, D. Fessa, K.V. Ryswyk, O. Hertel, M.S. Johnson, Particulate air pollution in the Copenhagen metro part 1: Mass concentrations and ventilation, *Environ. Int.*, 171 (2023) 107621. <https://doi.org/10.1016/j.envint.2022.107621>
- [3] L.T.N. Ngoc, Y. Lee, H.-S. Chun, J.-Y. Moon, J.S. Choi, D. Park, Y.-C. Lee, Correlation of α/γ -Fe₂O₃ nanoparticles with the toxicity of particulate matter originating from subway tunnels in Seoul stations, Korea, *J. Hazard. Mater.*, 382 (2020) 121175. <https://doi.org/10.1016/j.jhazmat.2019.121175>
- [4] H. Fang, S.D. Lowther, M. Zhu, C. Pei, S. Li, Z. Fang, X. Yu, Q. Yu, Y. Wang, Y. Zhang, K.C. Jones, X. Wang, PM_{2.5}-bound unresolved complex mixtures (UCM) in the Pearl River Delta region: Abundance, atmospheric processes and sources, *Atmos. Environ.*, 226 (2020) 117407. <https://doi.org/10.1016/j.atmosenv.2020.117407>
- [5] B. Gu, L. Zhang, M. Holland, M. Vieno, H.J.M. Van Grinsven, S. Zhang, S. Rao, M.A. Sutton, Particle toxicity's role in air pollution—Response, *Science*, 375 (2022) 506-507. <https://doi.org/10.1126/science.abn7647>
- [6] N. Nan, Z. Yan, Y. Zhang, R. Chen, G. Qin, N. Sang, Overview of PM_{2.5} and health outcomes: Focusing on components, sources, and pollutant mixture co-exposure, *Chemosphere*, 323 (2023) 138181. <https://doi.org/10.1016/j.chemosphere.2023.138181>
- [7] M.C. Turner, Z.J. Andersen, A. Baccarelli, W.R. Diver, S.M. Gapstur, C.A. Pope III, D. Prada, J. Samet, G. Thurston, A. Cohen, Outdoor air pollution and cancer: An overview of the current evidence and public health recommendations, *CA. Cancer. J. Clin.*, 70 (2020) 460-479. <https://doi.org/10.3322/caac.21632>
- [8] Y. Kim, Y.-H. Choi, M.K. Kim, H.J. Paik, D.H. Kim, Different adverse effects of air pollutants on dry eye disease: Ozone, PM_{2.5}, and PM₁₀, *Environ. Pollut.*, 265 (2020) 115039. <https://doi.org/10.1016/j.envpol.2020.115039>
- [9] G. Pereira, Cut particulate air pollution, save lives, *BMJ*, 375 (2021) n2561. <https://doi.org/10.1136/bmj.n2561>
- [10] H. Gao, W. He, Y.B. Zhao, D.M. Opris, G. Xu, J. Wang, Electret mechanisms and kinetics of electrospun nanofiber membranes and lifetime in filtration applications in comparison with corona-charged membranes, *J. Membr. Sci.*, 600 (2020) 117879. <https://doi.org/10.1016/j.memsci.2020.117879>
- [11] L. Ke, T. Yang, C. Liang, X. Guan, T. Li, Y. Jiao, D. Tang, D. Huang, S. Li, S. Zhang, X. He, H. Xu, Electroactive, Antibacterial, and Biodegradable Poly(lactic acid) Nanofibrous Air Filters for Healthcare, *ACS Appl. Mater. Interfaces*, (2023). <https://doi.org/10.1021/acsami.3c05834>
- [12] Y. Deng, T. Lu, X. Zhang, Z. Zeng, R. Tao, Q. Qu, Y. Zhang, M. Zhu, R. Xiong, C. Huang, Multi-

- hierarchical nanofiber membrane with typical curved-ribbon structure fabricated by green electrospinning for efficient, breathable and sustainable air filtration, *J. Membr. Sci.*, 660 (2022) 120857. <https://doi.org/10.1016/j.memsci.2022.120857>
- [13] Q. Sun, W.W.-F. Leung, Charged PVDF multi-layer filters with enhanced filtration performance for filtering nano-aerosols, *Sep. Purif. Technol.*, 212 (2019) 854-876. <https://doi.org/10.1016/j.seppur.2018.11.063>
- [14] C. Zhang, L. Yao, Z. Yang, E.S.-W. Kong, X. Zhu, Y. Zhang, Graphene Oxide-Modified Polyacrylonitrile Nanofibrous Membranes for Efficient Air Filtration, *ACS Appl. Nano Mater.*, 2 (2019) 3916-3924. <https://doi.org/10.1021/acsanm.9b00806>
- [15] Y. Li, L. Cao, X. Yin, Y. Si, J. Yu, B. Ding, Semi-Interpenetrating Polymer Network Biomimetic Structure Enables Superelastic and Thermostable Nanofibrous Aerogels for Cascade Filtration of PM2.5, *Adv. Funct. Mater.*, 30 (2020) 1910426. <https://doi.org/10.1002/adfm.201910426>
- [16] F.G. Torres, D.C. Dioses-Salinas, C.I. Pizarro-Ortega, G.E. De-la-Torre, Sorption of chemical contaminants on degradable and non-degradable microplastics: Recent progress and research trends, *Sci. Total Environ.*, 757 (2021) 143875. <https://doi.org/10.1016/j.scitotenv.2020.143875>
- [17] M. Tang, L. Jiang, C. Wang, X. Li, X. He, Y. Li, C. Liu, Y. Wang, J. Gao, H. Xu, Bioelectrets in Electrospun Bimodal Poly(lactic acid) Fibers: Realization of Multiple Mechanisms for Efficient and Long-Term Filtration of Fine PMs, *ACS Appl. Mater. Interfaces*, 15 (2023) 25919-25931. <https://doi.org/10.1021/acscami.3c02365>
- [18] J. Zhang, S. Gong, C. Wang, D.Y. Jeong, Z.L. Wang, K. Ren, Biodegradable Electrospun Poly(lactic acid) Nanofibers for Effective PM 2.5 Removal, *Macromol. Mater. Eng.*, 304 (2019) 1-8. <https://doi.org/10.1002/mame.201900259>
- [19] T.T. Le, E.J. Curry, T. Vinikoor, R. Das, Y. Liu, D. Sheets, K.T.M. Tran, C.J. Hawxhurst, J.F. Stevens, J.N. Hancock, O.R. Bilal, L.M. Shor, T.D. Nguyen, Piezoelectric Nanofiber Membrane for Reusable, Stable, and Highly Functional Face Mask Filter with Long-Term Biodegradability, *Adv. Funct. Mater.*, 32 (2022) 1-13. <https://doi.org/10.1002/adfm.202113040>
- [20] L. Wang, Y. Gao, J. Xiong, W. Shao, C. Cui, N. Sun, Y. Zhang, S. Chang, P. Han, F. Liu, J. He, Biodegradable and high-performance multiscale structured nanofiber membrane as mask filter media via poly(lactic acid) electrospinning, *J. Colloid Interface Sci.*, 606 (2022) 961-970. <https://doi.org/10.1016/j.jcis.2021.08.079>
- [21] D. Gao, R. Zhao, X. Yang, F. Chen, X. Ning, Bicomponent pla nanofiber nonwovens as highly efficient filtration media for particulate pollutants and pathogens, *Membranes*, 11 (2021). <https://doi.org/10.3390/membranes11110819>
- [22] L. Mei, Y. Ren, Y. Gu, X. Li, C. Wang, Y. Du, R. Fan, X. Gao, H. Chen, A. Tong, L. Zhou, G. Guo, Strengthened and Thermally Resistant Poly(lactic acid)-Based Composite Nanofibers Prepared via Easy Stereocomplexation with Antibacterial Effects, *ACS Appl. Mater. Interfaces*, 10 (2018) 42992-43002. <https://doi.org/10.1021/acscami.8b14841>
- [23] J. Liu, X. Qi, Q. Feng, Q. Lan, Suppression of Phase Separation for Exclusive Stereocomplex Crystallization of a High-Molecular-Weight Racemic Poly(l-lactide)/Poly(d-lactide) Blend from the Glassy State, *Macromolecules*, 53 (2020) 3493-3503. <https://doi.org/10.1021/acs.macromol.0c00112>
- [24] S. Zhao, H. Fan, N. Yin, T. Lin, S. Zhang, X. Xu, J. Ma, X. Zhu, Image binarization to calculate porosity of porous anodic oxides and derivation of porosity vs current, *Mater. Res. Bull.*, 93 (2017) 138-143. <https://doi.org/10.1016/j.materresbull.2017.04.031>
- [25] A. Ley, P. Altschuh, V. Thom, M. Selzer, B. Nestler, P. Vana, Characterization of a macro porous

- polymer membrane at micron-scale by Confocal-Laser-Scanning Microscopy and 3D image analysis, *J. Membr. Sci.*, 564 (2018) 543-551. <https://doi.org/10.1016/j.memsci.2018.07.062>
- [26] S. Li, R. Zhang, J. Xie, D.E. Sameen, S. Ahmed, J. Dai, W. Qin, S. Li, Y. Liu, Electrospun antibacterial poly(vinyl alcohol)/Ag nanoparticles membrane grafted with 3,3',4,4'-benzophenone tetracarboxylic acid for efficient air filtration, *Appl. Surf. Sci.*, 533 (2020) 147516. <https://doi.org/10.1016/j.apsusc.2020.147516>
- [27] Y. Liu, G. Ma, D. Fang, J. Xu, H. Zhang, J. Nie, Effects of solution properties and electric field on the electrospinning of hyaluronic acid, *Carbohydr. Polym.*, 83 (2011) 1011-1015. <https://doi.org/10.1016/j.carbpol.2010.08.061>
- [28] L. Mu, L. Zhang, J. Ma, K. Zhu, C. Chen, A. Li, Enhanced biometanization of waste polylactic acid plastic by mild hydrothermal pretreatment: Taguchi orthogonal optimization and kinetics modeling, *Waste Manage. (Oxford)*, 126 (2021) 585-596. <https://doi.org/10.1016/j.wasman.2021.03.044>
- [29] D. Pantaloni, A. Melelli, D.U. Shah, C. Baley, A. Bourmaud, Influence of water ageing on the mechanical properties of flax/PLA non-woven composites, *Polym. Degrad. Stab.*, 200 (2022) 109957. <https://doi.org/10.1016/j.polymdegradstab.2022.109957>
- [30] F. Iñiguez-Franco, R. Auras, G. Burgess, D. Holmes, X. Fang, M. Rubino, H. Soto-Valdez, Concurrent solvent induced crystallization and hydrolytic degradation of PLA by water-ethanol solutions, *Polymer*, 99 (2016) 315-323. <https://doi.org/10.1016/j.polymer.2016.07.018>
- [31] B. Wang, J. Yao, H. Wang, M. Wang, Construction of a ternary system: a strategy for the rapid formation of porous poly(lactic acid) fibers, *RSC Advances*, 12 (2022) 6476-6483. <https://doi.org/10.1039/D2RA00018K>
- [32] H.E. Gottlieb, G. Graczyk-Millbrandt, G.G.A. Inglis, A. Nudelman, D. Perez, Y. Qian, L.E. Shuster, H.F. Sneddon, R.J. Upton, Development of GSK's NMR guides – a tool to encourage the use of more sustainable solvents, *Green. Chem.*, 18 (2016) 3867-3878. <https://doi.org/10.1039/C6GC00446F>
- [33] A.d.P. Sánchez-Camargo, M. Bueno, F. Parada-Alfonso, A. Cifuentes, E. Ibáñez, Hansen solubility parameters for selection of green extraction solvents, *TrAC, Trends Anal. Chem.*, 118 (2019) 227-237. <https://doi.org/10.1016/j.trac.2019.05.046>
- [34] W.-L. Hung, D.-M. Wang, J.-Y. Lai, S.-C. Chou, On the initiation of macrovoids in polymeric membranes – effect of polymer chain entanglement, *J. Membr. Sci.*, 505 (2016) 70-81. <https://doi.org/10.1016/j.memsci.2016.01.021>
- [35] M. Alizadeh Sarami, M. Moghadam, A. Ghanadzadeh Gilani, Modified dielectric permittivity models for binary liquid mixture, *J. Mol. Liq.*, 277 (2019) 546-555. <https://doi.org/10.1016/j.molliq.2018.12.149>
- [36] S. Liu, M. Tyagi, P. Akcora, Polymer-Coupled Local Dynamics Enhances Conductivity of Ionic Liquids, *Macromolecules*, 53 (2020) 6538-6546. <https://doi.org/10.1021/acs.macromol.0c01434>
- [37] Z. Wang, C. Zhao, Z. Pan, Porous bead-on-string poly(lactic acid) fibrous membranes for air filtration, *J. Colloid Interface Sci.*, 441 (2015) 121-129. <https://doi.org/10.1016/j.jcis.2014.11.041>
- [38] W. Han, D. Rao, H. Gao, X. Yang, H. Fan, C. Li, L. Dong, H. Meng, Green-solvent-processable biodegradable poly(lactic acid) nanofibrous membranes with bead-on-string structure for effective air filtration: “Kill two birds with one stone”, *Nano Energy*, 97 (2022) 107237. <https://doi.org/10.1016/j.nanoen.2022.107237>
- [39] F. Liu, L. Wang, D. Li, Q. Liu, B. Deng, Preparation and characterization of novel thin film composite nanofiltration membrane with PVDF tree-like nanofiber membrane as composite scaffold, *Materials & Design*, 196 (2020) 109101. <https://doi.org/10.1016/j.matdes.2020.109101>
- [40] X. Cheng, Z. Zhang, L. Zhao, C. Deng, C. Li, Y. Du, M. Zhu, Multi-hierarchical nanofibre membranes

- composited with ordered structure/nano-spiderwebs for air filtration, *Journal of Environmental Chemical Engineering*, 11 (2023) 110561. <https://doi.org/10.1016/j.jece.2023.110561>
- [41] Z. Wang, C. Zhao, Z. Pan, Porous bead-on-string poly(lactic acid) fibrous membranes for air filtration, *J. Colloid Interface Sci.*, 441 (2015) 121–129. <https://doi.org/10.1016/j.jcis.2014.11.041>
- [42] H. Ozdemir, Mitigation impact of roadside trees on fine particle pollution, *Sci. Total Environ.*, 659 (2019) 1176-1185. <https://doi.org/10.1016/j.scitotenv.2018.12.262>
- [43] H. Wang, D. Zu, X. Jiang, Y. Xu, Z. Cui, P. Du, Z. Cheng, Z. Li, L. Li, C. Yang, X. Bai, B. Zhang, Y. Zhou, K. Wang, B. Li, Z. Huang, L. Zhao, B. Li, H. Wu, Bifunctional Activated Carbon Ultrathin Fibers: Combining the Removal of VOCs and PM in One Material, *Adv. Fiber. Mater.*, (2023). <https://doi.org/10.1007/s42765-023-00309-0>
- [44] Y. Yang, H. Wang, C. Wang, Y. Chen, B. Dang, M. Liu, X. Zhang, Y. Li, Q. Sun, Dual-Network Structured Nanofibrous Membranes with Superelevated Interception Probability for Extrafine Particles, *ACS Appl. Mater. Interfaces*, 15 (2023) 15036-15046. <https://doi.org/10.1021/acsami.3c01385>
- [45] C.W. Lou, S. Li, Y. Fan, T.-T. Li, X. Liu, L. Liu, B.-C. Shiu, J.-H. Lin, Preparation of antibacterial composite fiber membrane for air filtration with micro/nano structure, *J. Mater. Res. Technol.*, 24 (2023) 9949-9960. <https://doi.org/10.1016/j.jmrt.2023.05.075>
- [46] H. Liu, S. Zhang, L. Liu, J. Yu, B. Ding, A Fluffy Dual-Network Structured Nanofiber/Net Filter Enables High-Efficiency Air Filtration, *Adv. Funct. Mater.*, 29 (2019) 1904108. <https://doi.org/10.1002/adfm.201904108>
- [47] J. Song, B. Zhang, Z. Lu, Z. Xin, T. Liu, W. Wei, Q. Zia, K. Pan, R.H. Gong, L. Bian, Y. Li, J. Li, Hierarchical Porous Poly(l-lactic acid) Nanofibrous Membrane for Ultrafine Particulate Aerosol Filtration, *ACS Appl. Mater. Interfaces*, 11 (2019) 46261-46268. <https://doi.org/10.1021/acsami.9b18083>
- [48] Z. Xiong, J. Lin, X. Li, F. Bian, J. Wang, Hierarchically Structured Nanocellulose-Implanted Air Filters for High-Efficiency Particulate Matter Removal, *ACS Appl. Mater. Interfaces*, 13 (2021) 12408-12416. <https://doi.org/10.1021/acsami.1c01286>
- [49] H. Wang, H. Wang, X. Jin, H. Zhou, H. Wang, W. Wang, F. Ruan, Q. Feng, T. Lin, Tuning In-Plane Wicking Properties of Hydrophilic Fibrous Membranes Using Hydrophobic Fibrous Cover Layers, *Adv. Mater. Interfaces.*, 10 (2023) 2200741. <https://doi.org/10.1002/admi.202200741>
- [50] M. Nishikawara, T. Sako, H. Yokoyama, H. Yanada, Wicking characteristics of porous media using short copper micro/nanofibers, *Int. J. Heat Mass Transfer*, 195 (2022) 123137. <https://doi.org/10.1016/j.ijheatmasstransfer.2022.123137>
- [51] T. Liu, C. Cai, R. Ma, Y. Deng, L. Tu, Y. Fan, D. Lu, Super-hydrophobic Cellulose Nanofiber Air Filter with Highly Efficient Filtration and Humidity Resistance, *ACS Appl. Mater. Interfaces*, 13 (2021) 24032-24041. <https://doi.org/10.1021/acsami.1c04258>
- [52] Y. Zheng, H. Bai, Z. Huang, X. Tian, F.-Q. Nie, Y. Zhao, J. Zhai, L. Jiang, Directional water collection on wetted spider silk, *Nature*, 463 (2010) 640-643. <https://doi.org/10.1038/nature08729>
- [53] J. Zhang, X. Huang, Y. Xiong, W. Zheng, W. Liu, M. He, L. Li, J. Liu, L. Lu, K. Peng, Spider silk bioinspired superhydrophilic nanofibrous membrane for efficient oil/water separation of nanoemulsions, *Sep. Purif. Technol.*, 280 (2022) 119824. <https://doi.org/10.1016/j.seppur.2021.119824>
- [54] R. Shi, Y. Tian, L. Wang, Bioinspired Fibers with Controlled Wettability: From Spinning to Application, *ACS Nano*, 15 (2021) 7907-7930. <https://doi.org/10.1021/acsnano.0c08898>



1. A PLA electrospun fiber membrane with hierarchical structure was prepared
2. The applied solvent DMAC/DMC has a high degree of greenness
3. Membrane has high filtration efficiency, reduced pressure, excellent strength

Journal Pre-proofs

Declaration of interests

The authors declare that they have no known competing financial interests or personal relationships that could have appeared to influence the work reported in this paper.

Journal Pre-proofs

CRedit authorship contribution statement

Jing Ge: Data curation, Writing - original draft, Conceptualization, Visualization, Methodology.

Xujin Lv: Editing.

Jianwei Zhou: Editing.

Yarong Lv: Editing.

Jingyi Sun: Review & editing

Han Guo: Review & editing

Ce Wang: Review & editing

Ping Hu: Review & editing

Yong Liu: Supervision, Visualization, Investigation, Reviewing and Editing.

Journal Pre-proofs